THE JOURNAL OF PHYSICAL CHEMISTRY A
A JOURNAL OF THE AMERICAN CHEMICAL SOCIETY

pubs.acs.org/JPCA
Article

Transition-Metal Phthalocyanines as Versatile Building Blocks for Molecular Qubits on Surfaces

Corina Urdaniz,[§] Saba Taherpour,[§] Jisoo Yu, Jose Reina-Galvez, and Christoph Wolf*

Cite This: J. Phys. Chem. A 2025, 129, 2173−2181
Read Online

ABSTRACT: The search for molecular or colloidal building units capable of autonomously organized configurations has been a long-standing endeavor that has resulted in the development of innovative material categories, such as metal−organic and covalent organic or long-range molecular networks. In particular, the possibility of using molecules on surfaces to create specific architectures, for example, those containing nanostructures of S = 1/2 molecular spin, can enable versatile quantum materials and the exploration of future quantum devices. Transition-metal phthalocyanines are particularly attractive candidates as they are stable molecules that can host spin-bearing transition-metal ions in a planar conjugated ring. Here, we use density functional theory calculations to systematically study electronic and magnetic properties and hyperfine parameters for the whole series of 3d transition-metal atoms. We perform transport simulations of selected qubit candidates to further elucidate their suitability for molecular spin qubits on a surface.

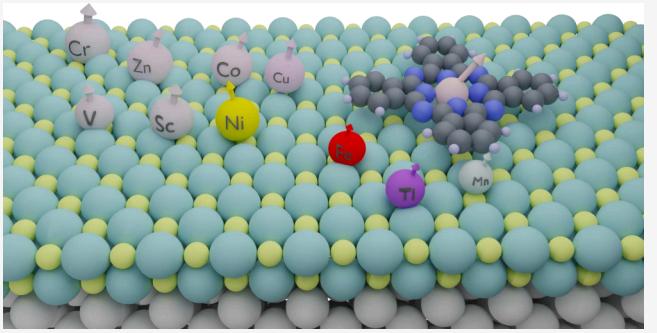

1. INTRODUCTION

The design of building blocks of molecular spins for assembly into complex systems has been a goal for quantum-coherent nanoscience.[1−5] Metal phthalocyanines (MPc, M = metal; Pc = $[C_8\ H_4\ N_2]_4$) have found widespread use in chemistry,[6] physics,[7,8] biology,[9] and others.[10] Their structural flexibility and delocalized π electrons create stable molecular frameworks with rich electronic behavior.[11,12] By manipulation of their molecular structure, it becomes feasible to prepare a robust environment for electron spins and drive an assembly of large numbers of qubits into atomically precise spin architectures.[13−19] The use of scanning tunneling microscopy (STM) coupled with scanning tunneling spectroscopy (STS) allows the probing of single molecular spins at atomic resolution.[20−24] Since the STM and STS techniques require a conducting substrate, the adsorbed molecule can interact strongly with the substrate through electron−electron scattering.[25] This process leads to a short lifetime of spins, which makes it difficult to determine the spin properties. To study the intrinsic properties of the molecule, it is essential to decouple the adsorbed species from the metallic substrate. This is commonly achieved by inserting a thin insulating layer between the metal substrate and the adsorbate.[26] In addition, thin dielectric layers on metal surfaces can alter the work function of the underlying metal substrate, therefore promoting or suppressing charge transfer.[27,28] In particular, experiments have shown that FePc becomes negatively charged when deposited on thin layers of magnesium oxide (MgO) deposited on silver (Ag), resulting in a $3d^7$ $(e_g)^4(b_{2g})^2(a_{1g})^1$ electron configuration with an effective electron spin of S = 1/2.[29,30] Similarly, for pentacene deposited on the same substrate, the entire molecule becomes singly negatively charged, giving rise to a SUMO/SOMO (singly unoccupied/occupied molecular orbital) type of system.[31,32]

We note that insulating layers are not the only approach to achieving a controlled charge transfer between molecules and metallic substrates. Molecular packing,[33] chemical ligand modification,[34] and the use of heterogeneous molecular bilayers[35] have also been demonstrated as viable routes. Among these, the use of thin insulating layers is particularly advantageous as it decouples the charge transfer mechanism from the molecules. This allows for the construction of both diffuse and densely packed molecular structures with well-defined charge transfer properties. A systematic study across the entire range of 3d transition-metal phthalocyanines (TMPcs) on Ag/MgO is, however, still lacking.

This work presents a first-principles study of the electronic and magnetic properties of TMPc for the whole 3d transition-metal row deposited on 2 monolayers (ML) of MgO on a Ag(100) substrate. We provide insight into the design of

Received: November 10, 2024
Revised: February 5, 2025
Accepted: February 7, 2025
Published: February 20, 2025

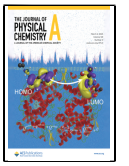

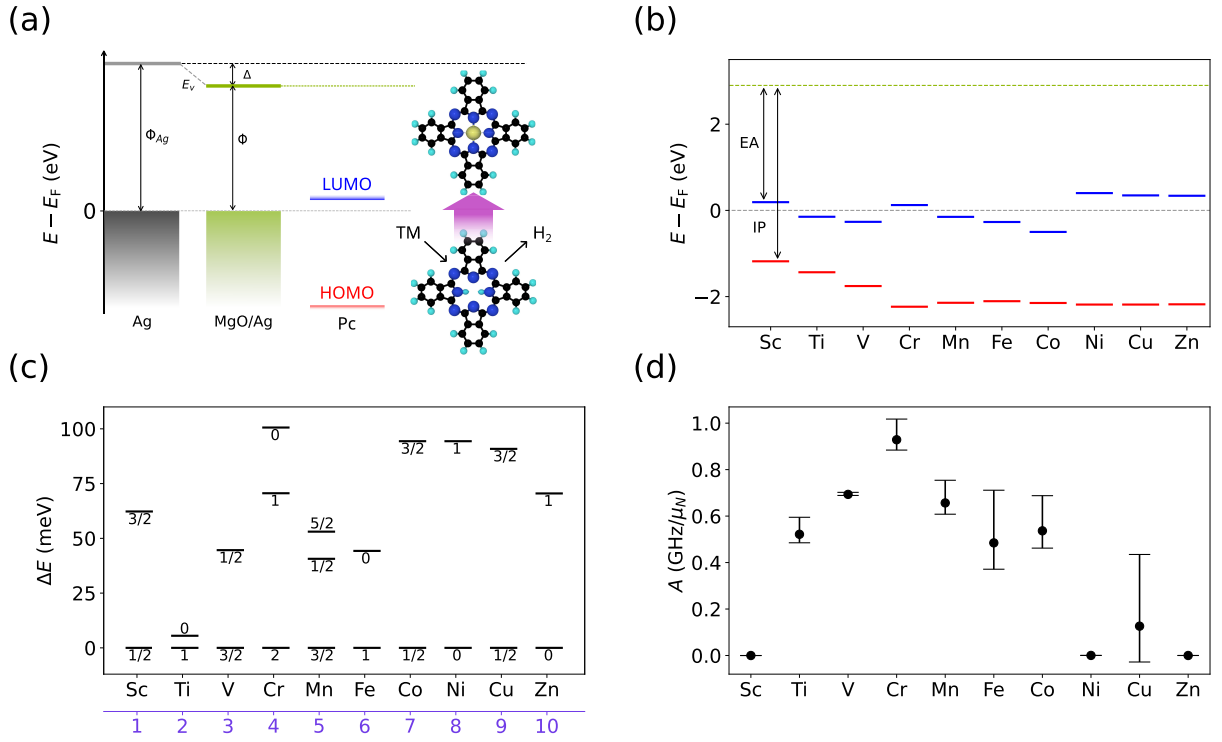

Figure 1. Properties of TMPc molecules in a vacuum: (a) Energy-level alignment model for TMPc molecules. The work function Φ_{Ag} of Ag(100) is reduced to Φ after the deposition of 2 ML of MgO by a shift Δ of the vacuum level (E_v). Shown are the HOMO and LUMO, solid blue and red lines, respectively, of a Pc molecule and the schematic transformation to a TMPc molecule by $H_2 \rightarrow$ TM exchange. (b) Energy-level alignment diagram from ΔSCF calculations of the TMPc molecules in the gas phase. IP = ionization potential and EA = electron affinity, their differences being the fundamental gap E_g. The green dashed line refers to the vacuum level. (c) Energy difference ΔE between possible spin configurations of each TMPc in a vacuum. The spin configurations with the lowest energy are taken as a reference. (d) Hyperfine coupling constants in GHz/μ_N for each TMPc in vacuum. The bars indicate the maximum and minimum values of the hyperfine tensor by summing isotropic (black dots) and dipolar contributions.

molecules on surfaces for spin-based qubits and the interplay between the metal substrate, insulating layer, and adsorbate.[36−38] Finally, we study the quantum-coherent properties of selected molecular spin qubits through nonequilibrium transport simulations.

2. COMPUTATIONAL METHODS

The calculations were perfomed using *ab initio* density functional theory (DFT) implemented in the Quantum Espresso package (version 7.1 or newer).[39,40] We used GBRV pseudopotentials,[41] and kinetic energy cutoffs for the wave functions and charge density were selected within a range of 70 to 140 Ry, depending on each transition metal (TM). The projector augmented wave (PAW) pseudopotentials from the PSLibrary[42] were used for the hyperfine calculations (details about the choice of pseudopotentials can be found in the Supporting Information). All calculations used the generalized gradient approximation of Perdew−Burke−Ernzerhof (GGA-PBE).[43] Integration of the Brillouin zone was performed by using only the gamma point, which was found to be sufficient to describe the system after convergence tests.

Two types of systems were considered: TMPc in the gas phase, for which we place the molecule in a large vacuum box, and TMPc adsorbed on Ag(100)/MgO. For the Ag(100)/MgO system, we consider a 5*5 lateral supercell of 2 ML of MgO and 2 ML of Ag(100). All cells were built by creating suitable lateral supercells of the relaxed simple unit cells and with 20 Å of vacuum in the out-of-plane z-direction. During the geometry optimization, the atomic positions of the molecular layer, the dielectric interlayer, and the first two metallic layers were allowed to relax. Van der Waals interactions were treated using the revised VV10 (rVV10) functional. We used rVV10 as it is the most dependable dispersion correction for systems featuring mixed bonding environments.[44] For hyperfine calculations, we used the GIPAW formalism and X-ray absorption spectra were calculated using the XSpectra code, both implemented in Quantum Espresso.[45−49]

ΔSCF calculations were performed by calculating the total energy of the neutral N-electron molecule and the total energy of the $N + 1$ (or $N - 1$) anionic (cationic) molecule. This difference is the total energy when adding (or removing) an electron and is therefore the electron affinity (EA = $E_N - E_{N+1}$) or ionization energy (IP = $E_N - E_{N-1}$). This method is applied to the geometry of the neutral molecule.

For nonequilibrium transport simulations of electron-spin resonance spectra and open quantum system dynamics, we used a Green's function formalism. The model consists of a single-orbital Anderson impurity coupled to a left and right lead via time-dependent hopping operators. If one of the electrodes is polarized, then the time-dependent hopping in resonance with the Zeeman-split spin states leads to coherent Rabi oscillations and decoherence.[50−52]

3. RESULTS

Before discussing the effects of adsorption on the electronic and magnetic molecular structure, we briefly present the chemical configuration of TMPc in the gas phase as well as the

https://doi.org/10.1021/acs.jpca.4c07627
J. Phys. Chem. A 2025, 129, 2173−2181

Table 1. Ionization Potential (IP), Electron Affinity (EA), Transport Gap ($E_g^{tr.}$ = IP − EA), and Optical Gap ($E_g^{opt.}$) for the TMPc Series (in eV)[65a]

	Sc	Ti	V	Cr	Mn	Fe	Co	Ni	Cu	Zn
IP	4.08	4.33	4.65	5.13	5.04(4.5)	5.01(5.1)	5.05(4.4)	5.08(5.1)	5.08(5.0)	5.08(5.1)
EA	2.71	3.05(3.55)	3.16	2.78	3.05	3.17	3.40	2.50	2.55	2.56
$E_g^{tr.}$	1.37	1.28	1.49	2.35	1.99	1.84	1.65	2.58	2.53	2.52
$E_g^{opt.}$	1.8[12]	NA	NA	1.80[59]	1.2[60]	1.2[59]	1.60[61]	1.68[62]	1.64[63]	1.74[64]

[a]IP, EA, and $E_g^{tr.}$ were obtained from the ΔSCF calculations with literature values where available in parentheses.[65] The $E_g^{opt.}$ was obtained from data available in the experimental literature. NA = no data available.

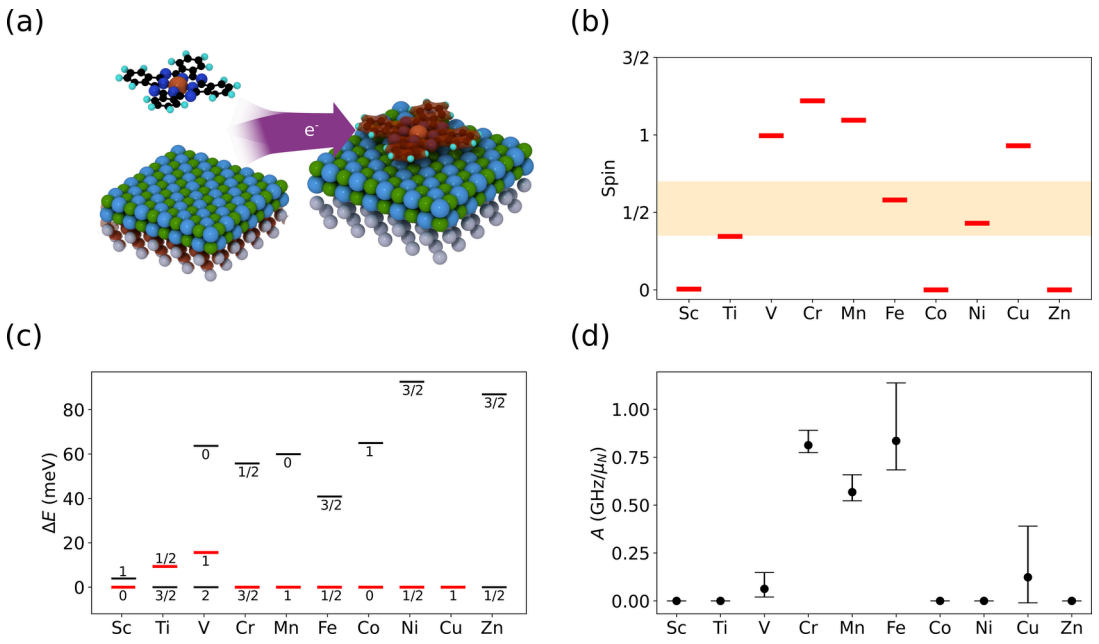

Figure 2. Magnetic properties of TMPc on Ag/MgO: (a) Schematic of a TMPc molecule adsorbing on 2 ML of MgO and undergoing charge transfer (charge difference is shown with iso = 0.07). (b) Final spin state of each TMPc after adsorption. (c) Energy difference ΔE between possible spin configurations of each $[TMPc]^{-1}$ in vacuum and their lowest-energy state. Red lines indicate the spin state assumed in panel (b). (d) Hyperfine coupling constants in GHz/μ_N for each TMPc on Ag/MgO. The bars indicate the maximum and minimum values of the hyperfine tensor by summing isotropic (black dots) and dipolar contributions.

spin state and the value of the hyperfine constant that we will refer to as the vacuum states later as reference.

3.1. Properties of Neutral TMPc Molecules in Vacuum. Phthalocyanines ($[C_8\ H_4\ N_2]_4\ H_2$) are flat molecules in which two hydrogen atoms are surrounded by an organic ligand. This molecule can be easily modified by exchanging the central H_2 with a 3*d* transition metal, with the resulting molecule referred to as TMPc in the following. In TMPc, the central TM ion is coordinated with four nitrogen atoms, exhibiting D_{4h} symmetry, as shown in Figure 1(a), which formally gives the TM atom a 2+ chemical oxidation state. Figure 1(a) also shows the alignment of the highest occupied molecular orbital (HOMO) and lowest unoccupied molecular orbital (LUMO) of a Pc molecule with the Fermi level of the Ag(100) substrate capped by 2 ML of MgO. Upon depositing 2 ML of MgO on Ag(100), the work function of Ag(100) is reduced by Δ due to a shift in the vacuum level. This brings the Fermi level of the substrate closer to the LUMO of the Pc molecule.

We performed ΔSCF calculations for the entire series of TMPcs to determine their respective ionization potential (IP) and electron affinity (EA). The results of the ΔSCF calculation shown in Figure 1(b) anticipate that all molecules are likely to undergo charge transfer from the substrate to the LUMO upon adsorption on Ag/MgO. When the EA or the IP lies close to the work function of Ag/MgO, the molecule can change its charge state by forming an anion or cation. We note that this model does not capture all possible contributions that lead to charge transfer;[31,53,54] however, based on this simple model, VPc, FePc, and CoPc are the most likely to undergo charge transfer by forming VPc^{-1}, $FePc^{-1}$, and $CoPc^{-1}$, followed by the other TMPcs. As we will show later, all TMPc molecules with the exception of ZnPc ($3d^{10}$) do eventually become anionic once deposited on Ag/MgO. We note that the small variation of the IP is in line with previous experimental studies.[55] In Table 1, we summarize the results of our calculations related to IP, EA, and the transport gap $E_g^{tr.}$ = IP − EA. We include literature values for the optical gap of each TMPc (where available) since the optical gap is widely available in the experimental literature. Due to the exciton binding energy E_{ex} of typically less than 1 eV,[56] the optical gap $E_g^{opt.} = E_g^{tr.} - E_{ex}$ is a useful reference for the lower bound of the transport gap.[57,58]

Molecular spin qubits can utilize electron[66−68] as well as coupled electron−nuclear[69,70] spin systems. First, we discuss the electron-spin states *S* of TMPc in vacuum. Figure 1(c) shows the spin ground state as well as the excited spin states with their respective energies for the neutral TMPc molecule.

https://doi.org/10.1021/acs.jpca.4c07627
J. Phys. Chem. A 2025, 129, 2173−2181

We observed that for complexes with TM from Ti to Fe, the high-spin configuration is preferred, while those formed with Co and Ni favor the low-spin configuration. As expected, Sc ($3d^1 4s^0$) and Cu ($3d^9 4s^0$) prefer the low-spin $S = 1/2$ configuration. Second, we assess the possibility of measuring the nuclear spin states I via electronic spin by calculating the hyperfine tensor A. The hyperfine tensor consists of isotropic and dipolar contributions, $A = A_{iso} + T$. The dipolar part has an anisotropic spatial dependence. To visualize both in a rather simple way, we plotted the minimum and maximum of A. The magnitude of the hyperfine interactions is important for efficiently coupling the electron and nuclear spins. The larger the hyperfine coupling, the more efficiently the nuclear spin can be controlled through the electron spin. Further, larger hyperfine coupling constants also lead to wider spacing in the ESR spectrum, which allows addressing of each transition at the experimentally set ESR line width. Figure 1(d) presents the values obtained for the hyperfine coupling constants in GHz/μ_N for TMPc in vacuum. In magnitude, for V, Cr, Mn, and Fe the values are nearly identical. Similarly, Sc, Co, and Cu also exhibit comparable values, though these values are significantly lower. This discrepancy can likely be attributed to variations in s-orbital occupation. Combining Figure 1(c and d) suggests that CoPc would make an excellent candidate for an $S = 1/2$ spin qubit with strong hyperfine coupling. ^{59}Co also has a nuclear spin of $I = 7/2$, making it an electron−nuclear-coupled spin-qudit candidate with a large Hilbert space. Last we note that, to the best of our knowledge, TiPc has not been synthesized; however, its oxidized variant titanyl phthalocyanine (TiOPc) is widely discussed in the literature.[71]

3.2. Properties of TMPc Adsorbed on 2 ML MgO/Ag(001). To study the properties of spins deposited on surfaces, a thin dielectric layer is inserted between the conductive metal substrate and the spin to reduce scattering from the substrate and therefore increase the lifetime and coherence time of the adsorbed spin. Here, we consider a substrate of silver(100) capped by two layers of MgO. This system is well understood and used in several studies.[26,32] It has been shown by calculations and experiments that MgO reduces the work function of bare Ag(100) ($\Phi = 4.7$ eV) by 1 eV for the first layer of MgO and by 1.3 eV for the second layer, after which it remains approximately constant.[72,73] This reduction of the work function brings the LUMO of all TMPcs close to the Fermi level of the substrate system, which enables charge transfer from the silver to the molecules.

In Figure 2, we study the effect that adsorption on Ag/MgO has on the magnetic properties of TMPc molecules. Figure 2(a) shows a schematic of charge transfer from the Ag substrate to the TMPc molecule upon adsorption. The resulting spin state is shown in Figure 2(b). The change in spin state with respect to Figure 1(c) indicates that all molecules, with the exception of ZnPc, undergo charge transfer and form their singly charged anionic form $[TMPc]^{-1}$. This is confirmed by calculations of the anionic species $[TMPc]^{-1}$ molecule in a vacuum as shown in Figure 2(c), which shows the lowest and excited spin states for all anionic TMPcs.

Focusing on $S = 1/2$ from Figure 2(b and c) $[FePc]^{-1}$ and $[NiPc]^{-1}$ are candidates for $S = 1/2$ molecular spin qubits. Higher spin systems are also available in the TMPc series, with $S = 1$ VPc, CrPc, and MnPc, while our calculations suggest a quenched spin ground state on ScPc, TiPc, CoPc, NiPc, and ZnPc. For all quenched moment, TMPc magnetic excited states exist due to the fact that they have non-zero $3d$ occupancy; however, the competition between electron−electron repulsion the square-planar crystal field can lead to a nonmagnetic ground state. As shown in Figure 2(c), not all ionic species obtain the same spin ground state in a vacuum compared to the adsorbed TMPc. We confirmed that this is not driven by distortions of internal degrees of freedom of the molecule, which remain very small throughout the entire TMPc series (Figures S2 and S4). To focus on an example, we can discuss $[ScPc]^0$, $[ScPc]^{-1}$, and ScPc/Ag/MgO. $[ScPc]^0$ has an electron configuration of $3d^1 4s^0 L^0$ with a ground state of $S = 1/2$. When in its anionic state, $[ScPc]^{-1}$ becomes $3d^2 4s^0 L^0$, with its ground state being $S = 0$ and its excited state $S = 1$ lying roughly 5 meV higher. This excited-state splitting should be relevant for inelastic spin excitation spectroscopy and could be used to identify the spin ground and excited states in the experiment.[74] When adsorbed on Ag/MgO, ScPc is to good approximation $3d^2 4s^0 L^0$, i.e., the same as $[ScPc]^{-1}$. According to Figure 1(b), NiPc, CuPc, and ZnPc are less likely to undergo charge transfer; however, the resulting ground states of the respective NiPc and CuPc on Ag/MgO reflect the TMPc anionic molecules of Figure 2(c) and only ZnPc remains neutral and assumes the spin configuration of Figure 1(c). We now turn to FePc and CoPc, which should undergo charge transfer based on their EA position relative to the Fermi level of the substrate. FePc, which is the best studied of the TMPcs considered here, does undergo a charge transfer of $3d^6 4s^0 L^0$ ($S = 1$) → $3d^7 4s^0 L^0$ ($S = 1/2$) in agreement with the experiment. CoPc is an analogous case with a nonmagnetic ground state on Ag/MgO akin to its $[CoPc]^{-1}$ state.

We calculated the adsorption height and adsorption energy of TMPc adsorbed on the O-top site of MgO and with the characteristic (2, 1) rotation of the ligand found in the experiment.[29] The adsorption height $h_{ads} = TM_z - O_z$ denotes the vertical distance between the z-coordinate of the TM and the closest oxygen atom which falls between 2 and 3 Å and seems to be shorter for the beginning of the $3d$ TM row compared to the end. (See Figure S2 and Table S2 for details.) A similar trend is observed for the adsorption energy ($E_{ads} = E_{total} - E_{Ag/MgO} - E_{TMPc}$), which falls between 4 and 7 eV (Figure S2), which is generally in line with values measured for TMPc on a metallic surface.[75] This indicates that the interaction of Ti and V with the underlying O is stronger compared to that of the later TM ions, in line with the strong tendency of Ti and V to form titanyl and vanadyl groups.[76−78] We note that experiments have shown that FePc diffuses or rotates on the surface with a much lower activation energy (<0.5 eV) than the adsorption energy; i.e., the structurally limiting energy scale is not set by the adsorption energy.[29,79] To experimentally identify the adsorbed species and the spin states, we provide simulated X-ray absorption spectra for the K-edge and L_2-edge for each TMPc (Figures S8 and S9).[48,49] Finally, we calculated the hyperfine coupling for the adsorbed molecules, as shown in Figure 2(d), to explore the possibility of combined electron-spin nuclear-spin quantum bits. Here, $[FePc]^{-1}$ emerges as a candidate for the $S = 1/2$ and $I = 1/2$ electron−nuclear qudit, while $[TiPc]^{-1}$ and $[NiPc]^{-1}$ (both $S = 1/2$) have vanishing electron−nuclear coupling strength.

3.3. Nuclear Spin−Electron Spin Combined Qudits. We now assess the possibility of creating molecular qudits by combining the nuclear spin I with an electron spin $S = 1/2$ system using the hyperfine tensor $\underline{A}$ which couples S and I by $\hat{H} = S \cdot \underline{A} \cdot I$. In such a system, the nuclear spin represents the quantum bit while the electron spin can be used to drive and

https://doi.org/10.1021/acs.jpca.4c07627
J. Phys. Chem. A 2025, 129, 2173−2181

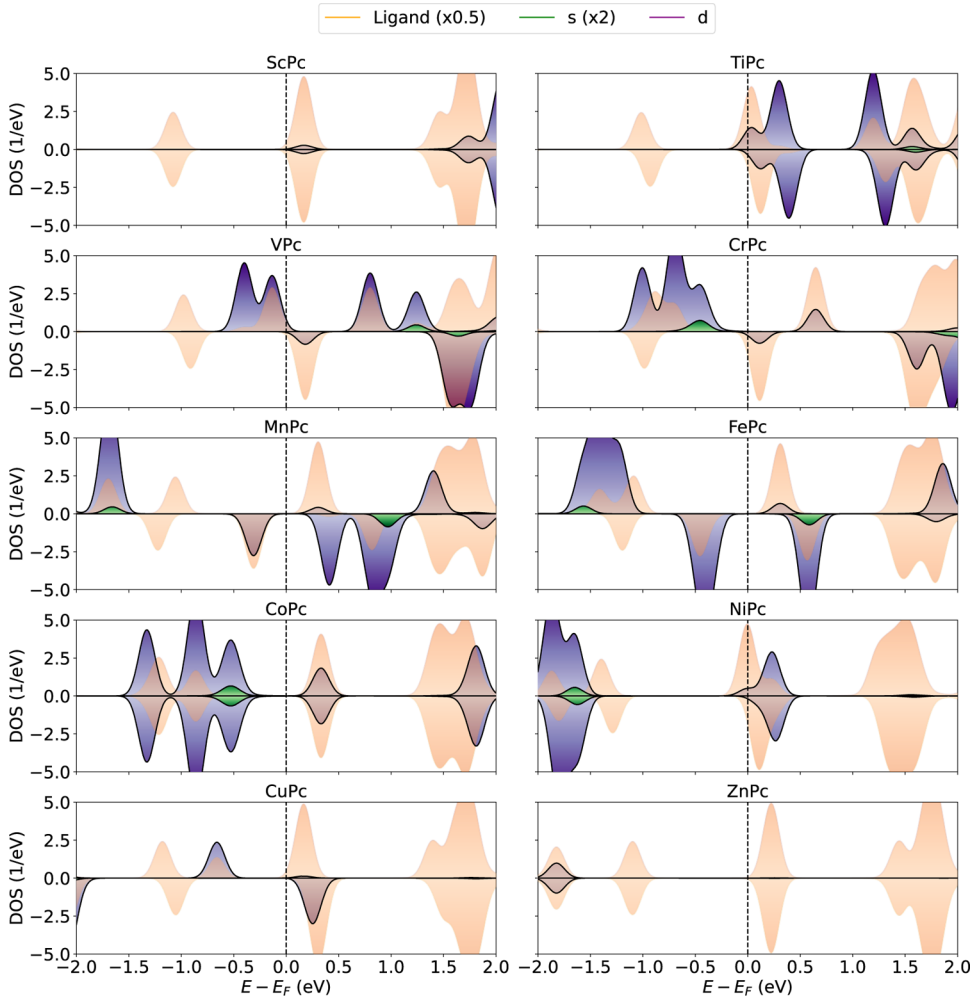

Figure 3. Density of states of adsorbed TMPc molecules. Each panel corresponds to the DOS plot for a TMPc molecule adsorbed on Ag/MgO with the individual contributions color coded for the TM ion (s and d orbitals) and the macrocycle (ligand).

read-out the quantum state of the nucleus. We will focus here on systems with $S = 1/2$, but the same logic applies to larger spin systems. Further, we will focus on systems where the hyperfine coupling strength $\underline{A}$ exceeds the typical line width of the ESR signal of about $\Gamma = 30$ MHz,[80] at least along some direction of the anisotropic hyperfine coupling tensor. The results of hyperfine calculations of TMPc on Ag/MgO are shown in Figure 2(d). Immediately four systems stand out for having large hyperfine coupling: VPc, CrPc, MnPc, and FePc. Out of these, only FePc is $S = 1/2$ (cf. Figure 2(b)). Fe has several stable isotopes with the following nuclear spins: ^{56}Fe ($I = 0+$), ^{57}Fe ($I = 1/2-$), ^{58}Fe ($I = 0+$), which allows the design of an $S = 1/2$, $I = 1/2$ qubit by utilizing isotopically purified ^{57}Fe since the natural abundance of this isotope is only around 2%. With a nuclear gyromagnetic factor of $g \approx 0.18$,[81] a splitting of the nuclear spin states of $\delta f \approx 1100$ MHz can be expected, which is well within the typical bandwidth of an ESR-STM.

Other TMPcs that could be $S > 1/2$ qudit candidates are MnPc with $S = 1$ (^{55}Mn, $I = 5/2$) or CrPc with $S = 3/2$ (^{53}Cr, $I = 3/2$). However, their larger electron spins might make these systems less suitable for pilot studies as they massively increase the complexity of driving and detecting the ESR signal. Simulated hyperfine spectra for all TMPc molecules with non-zero electron spin and stable isotopes with non-zero nuclear spin can be found in Figure S10 with values from Table S5.

The trend in the Fermi contact contribution of the hyperfine coupling strength can be related to the 4*s* polarization.[82] To analyze this, we calculated the density of states (DOS) projected onto the *s*, *d*, and ligand manifolds of the molecule. The data is shown in Figure 3, and the individual contributions are also listed in Table S4. By contrasting the DOS of the adsorbed molecule and the neutral (Figure S5) and anionic (Figure S6) TMPcs in vacuum, we can further confirm that all TMPcs with the exception of ZnPc undergo charge transfer when adsorbed on Ag/MgO. Further, the DOS emphasizes the different possible contributions to the total spin of the molecule. In most cases, the majority of the polarization is localized on the central TM ion, which is in line with STS studies on FePc on Ag/MgO.[29] MnPc and FePc are interesting cases, as they both acquire ligand polarizations that make them antiferromagnetically coupled to the *d*-shell, therefore reducing the overall spin of the molecule to $S = 1$ and $S = 1/2$, respectively. NiPc also results in $S = 1/2$, but its polarization is predominantly on the ligand, highlighting the distinct distribution of spin density between these two systems (Figure S7).

3.4. Simulated ESR Spectra. Finally, we turn to the question of quantum-coherent properties of TMPc molecules

https://doi.org/10.1021/acs.jpca.4c07627
J. Phys. Chem. A 2025, 129, 2173−2181

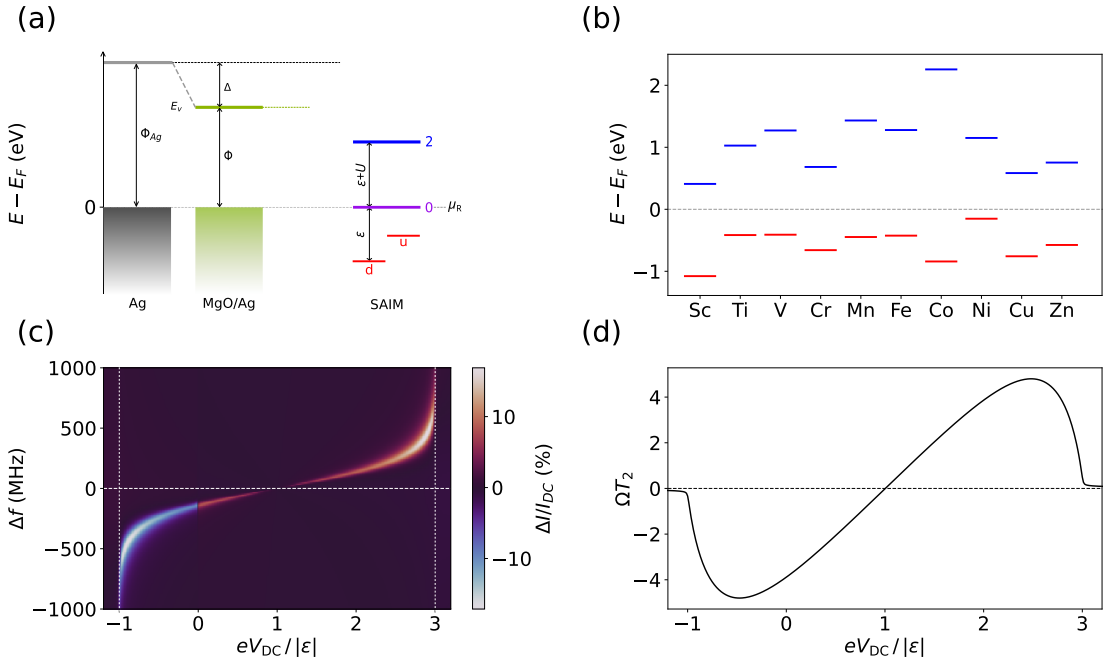

Figure 4. Transport properties of TMPc molecules on Ag/MgO. (a) SAIM as utilized in our simulations, indicating the charging energies ε and $\varepsilon + U$ and the chemical potential of the right electrode $\mu_R = 0$. (b) Values for ionization energy ε and charging energy U obtained from ΔSCF calculations of the TMPcs in their anionic states and (c) simulated ESR spectra shown as 2D color maps for FePc on Ag/MgO as a function of the DC bias. (d) Spin-qubit figure of merit ΩT_2 as a function of the DC bias. Other parameters used in the calculation: $g = 2$ isotropic, $B = 0.6$ (sin θ, 0, cos θ) T, $\theta = 20°$, $T = 1.4$ K, $\gamma_L = \gamma_R = 5$ μeV, $A_L = 0.5$ and $P_L = 0.6$, and A_R, $P_R = 0$.

Table 2. Impurity Parameters ε and U of TMPc Series (in eV)[a]

	Sc	Ti	V	Cr	Mn	Fe	Co	Ni	Cu	Zn
ε	−1.078	−0.416	−0.410	−0.659	−0.447	−0.425	−0.841	−0.152	−0.758	−0.575
U	1.487	1.443	1.681	1.342	1.879	1.703	3.134	1.302	1.342	1.329

[a]Given are the values that enter the transport simulation.

adsorbed on Ag/MgO. In the following, we will address the question of the suitability of these molecules as $S = 1/2$ qubits. Of particular interest are the achievable Rabi rate Ω, the coherence time T_2, and the signal intensity, which we take as on-resonant current divided by the background current or off-resonance current ($\Delta I^{ESR}/I_{DC} = (I^{ESR} - I_{DC})/I_{DC}$), where DC denotes the background current. To model the transport, we use the single Anderson impurity model (SAIM) connected to a left (L) and right (R) electrode with chemical potentials $\mu_{L,R}$ via hoppings that are harmonically modulated on resonance with an ESR transition, as a consequence of the modulation of the chemical potential of the leads or a barrier modulation.[50,83−85] This model has been used previously to successfully simulate ESR in single-atom ESR on Ti on Ag/MgO[51,52,86] and FePc adsorbed on Ag/MgO.[87] To characterize the impurity, we map the results of another ΔSCF calculations, namely, the IP and EA on the SAIM. This is possible due to the fact that IP (EA) corresponds to the energy to remove (add) one electron to the $[TMPc]^{-1}$ molecule. In Figure 4(a), in contrast to the ΔSCF calculations in Figure 1(b), the reference state is the singly charged molecule $[TMPc]^{-1}$, and the charge states that entered the ΔSCF calculations are $[TMPc]^{0}$ and $[TMPc]^{-2}$. We use the work function of bare silver reduced by the capping layer of 2 ML of MgO as used previously and fix the 0-charge state (empty state) of the SAIM to the Fermi level, which is also the chemical potential of the right electrode μ_R, set to zero in the model.

The energy needed to remove one electron from the impurity level to the Fermi energy of the electrode is IP $- E_F$ and yields ε = IP $- E_F + \Delta$ while the energy to put two electrons in the SAIM is $2\varepsilon + U = E_F - \Delta -$ EA. A summary of the impurity energy levels can be found in Figure 4(b) and Table 2. For the actual ESR simulation, we focus on the effective $S = 1/2$ FePc that could be used as molecular spin qubits. FePc is characterized by $\varepsilon = -0.425$ eV and $U = 1.703$ eV, which are generally in agreement with values obtained from recent experiments.[87]

A representative spectrum as a function of the DC bias $eV_{DC} = \mu_L - \mu_R = \mu_L$ is shown in Figure 4(c) for FePc. The ESR spectrum shows a nonlinear shift in resonance frequency f_0 as the magnitude of V_{DC} is increased. Close to the charging energies (-1, $1 + U/\varepsilon$ in units of ε), the shifting increases logarithmically, and then the signal vanishes when the DC bias crosses the charging thresholds. This behavior is yielded by the qubit quality factor ΩT_2 as shown in Figure 4(d). Within the charging window, the transport operates in the so-called Coulomb blockade regime of SAIM, where the spin can exhibit quality factors of as high as nearly 5. However, outside this charging window, the quality factor drastically drops to values close to zero as the system transitions to the sequential regime. In sequential transport and under the right conditions, the model still yields a measurable ESR signal; however, the spin

https://doi.org/10.1021/acs.jpca.4c07627
J. Phys. Chem. A 2025, 129, 2173−2181

consistently displays overdamped behavior in this regime (Figure S11).[52]

The quality factor depends on charging energy values, couplings, and the lifetime of energy levels as well as polarization P_α and driving amplitude A_α, where $\alpha = L$ and R denotes the left and right electrodes, respectively. Although the actual dependence of the decoherence time T_2 is strongly influenced by the transport regime, whether sequential or cotunneling, the Rabi flip-flop rate behavior remains unchanged, as it depends solely on the charging energies for a given coupling and driving and polarization of the tip on top of the magnetic direction.[50−52] Therefore, when focusing on enhancing the quality factor for a given impurity, the primary goal is to improve the spin-qubit's coherence time, assuming that the Rabi rate has been maximized. Due to the low value of ϵ for NiPc, it is not easily possible to achieve a large quality factor, making it a less promising candidate for a molecular spin qubit.

4. CONCLUSIONS

We investigated the behavior of transition-metal phthalocyanines adsorbed on a 2 ML MgO/Ag(001) substrate. The charge transfer from the substrate to the TMPc leads to the formation of charged anionic species $[TMPc]^{-1}$, altering the spin states and suggesting the viability of certain TMPcs such as TiPc and FePc as candidates for $S = 1/2$ molecular spin qubits. NiPc, on the other hand, with $S = 1/2$, is most likely less viable due to its low ionization energy. VPc, CrPc, MnPc, and CuPc all exhibit $S > 1/2$, which allows building more complex spin systems or molecular electron-spin qudits. If one considers the nuclear spin degree of freedom, then FePc emerges as an ideal prototypical $S = 1/2$, $I = 1/2$ with large hyperfine splitting. NiPc stands out, with the unpaired spin being located almost entirely on the ligand. This could enhance the ligand-mediated coupling of molecular complexes including NiPc as an intermediate between two magnetic spin centers. ScPc, CoPc, and ZnPc are non-magnetic, which makes them ideal iso-structural spacers to decouple spin-breaking phthalocyanine molecules. In summary, we have provided a comprehensive overview of the magnetic, electronic, and hyperfine properties of TMPcs for the 3*d* series. Our work demonstrates the potential of TMPc molecules as building blocks for molecular spin qubits and electron−nuclear spin qudits and highlights the dual role of the substrate to decouple the spin from the conduction electrons and to facilitate charge transfer to achieve a desired spin state. By proper selection of the substrate and adsorbate, a wide range of spin states can be engineered using TMPcs on surfaces. We believe our findings can help guide the selection of appropriate building blocks for quantum spin systems on surfaces.

■ ASSOCIATED CONTENT

Data Availability Statement

The data supporting the findings of this study are available from the corresponding author upon reasonable request.

Supporting Information

The Supporting Information is available free of charge at https://pubs.acs.org/doi/10.1021/acs.jpca.4c07627.

Additional figures (ZIP)

Details for the DFT calculation; structural analysis of the TMPc molecules in vacuum and after adsorption; simulated hyperfine and X-ray absorption spectra and additional calculations for nonequilibrium transport (PDF)

■ AUTHOR INFORMATION

Corresponding Author

Christoph Wolf − *Center for Quantum Nanoscience, Institute for Basic Science (IBS), Seoul 03760, Korea; Ewha Womans University, Seoul 03760, Korea;* orcid.org/0000-0002-9340-9782; Email: wolf.christoph@qns.science

Authors

Corina Urdaniz − *Center for Quantum Nanoscience, Institute for Basic Science (IBS), Seoul 03760, Korea; Ewha Womans University, Seoul 03760, Korea;* orcid.org/0009-0003-4139-0236

Saba Taherpour − *Center for Quantum Nanoscience, Institute for Basic Science (IBS), Seoul 03760, Korea; Department of Physics, Ewha Womans University, Seoul 03760, Korea;* orcid.org/0009-0006-6738-4397

Jisoo Yu − *Center for Quantum Nanoscience, Institute for Basic Science (IBS), Seoul 03760, Korea; Department of Physics, Ewha Womans University, Seoul 03760, Korea*

Jose Reina-Galvez − *Center for Quantum Nanoscience, Institute for Basic Science (IBS), Seoul 03760, Korea; Ewha Womans University, Seoul 03760, Korea*

Complete contact information is available at: https://pubs.acs.org/10.1021/acs.jpca.4c07627

Author Contributions

[§]C.U. and S.T. contributed equally to this work.

Notes

The authors declare no competing financial interest.

■ ACKNOWLEDGMENTS

We acknowledge fruitful discussions with L. Colazzo, N. Lorente, and P. Josse during the writing of this manuscript. This work was supported by the Institute for Basic Science (IBS-R027-D1).

■ REFERENCES

(1) Chen, Y.; Bae, Y.; Heinrich, A. J. Harnessing the quantum behavior of spins on surfaces. *Adv. Mater.* **2023**, *35*, 2107534.

(2) Wang, Y.; Haze, M.; Bui, H. T.; Soe, W.-h.; Aubin, H.; Ardavan, A.; Heinrich, A. J.; Phark, S.-h. Universal quantum control of an atomic spin qubit on a surface. *npj Quantum Information* **2023**, *9*, 48.

(3) Blinov, B. B.; Leibfried, D.; Monroe, C.; Wineland, D. J. Quantum computing with trapped ion hyperfine qubits. *Quantum Information Processing* **2004**, *3*, 45−59.

(4) Thiele, S.; Balestro, F.; Ballou, R.; Klyatskaya, S.; Ruben, M.; Wernsdorfer, W. Electrically driven nuclear spin resonance in single-molecule magnets. *Science* **2014**, *344*, 1135−1138.

(5) Vincent, R.; Klyatskaya, S.; Ruben, M.; Wernsdorfer, W.; Balestro, F. Electronic read-out of a single nuclear spin using a molecular spin transistor. *Nature* **2012**, *488*, 357−360.

(6) Liu, Z.; Zhang, X.; Zhang, Y.; Jiang, J. Theoretical investigation of the molecular, electronic structures and vibrational spectra of a series of first transition metal phthalocyanines. *Spectrochimica Acta Part A: Molecular and Biomolecular Spectroscopy* **2007**, *67*, 1232−1246.

(7) Shirai, H.; Maruyama, A.; Kobayashi, K.; Hojo, N.; Urushido, K. Functional metal-porphyrazine derivatives and their polymers, 4. Synthesis of poly(styrene) bonded Fe(III)- as well as Co(II)-4,4',4",4‴-tetracarboxyphthalocyanine and their catalase-like activity. *Makromol. Chem.* **1980**, *181*, 575−584.

(8) Furuya, N.; Yoshiba, H. Electroreduction of nitrogen to ammonia on gas-diffusion electrodes modified by metal phthalocyanines. *Journal of electroanalytical chemistry and interfacial electrochemistry* **1989**, *272*, 263−266.
(9) Grobosch, M.; Schmidt, C.; Kraus, R.; Knupfer, M. Electronic properties of transition metal phthalocyanines: The impact of the central metal atom (d5-d10). *Org. Electron.* **2010**, *11*, 1483−1488.
(10) Gregory, P. Industrial applications of phthalocyanines. *J. Porphyrins Phthalocyanines* **2000**, *04*, 432.
(11) Leznoff, C. C.; Lever, A. B. P. *Phthalocyanines: Properties and Applications*; VCH: New York, 1989.
(12) Guilard, R.; Kadish, K. M.; Smith, K. M.; Guilard, R. *The Porphyrin Handbook*; Academic Press: New York, 2003; Vol. *18*.
(13) Gaita-Ariño, A.; Luis, F.; Hill, S.; Coronado, E. Molecular spins for quantum computation. *Nature Chem.* **2019**, *11*, 301−309.
(14) Atzori, M.; Sessoli, R. The second quantum revolution: role and challenges of molecular chemistry. *J. Am. Chem. Soc.* **2019**, *141*, 11339−11352.
(15) Graham, M. J.; Zadrozny, J. M.; Fataftah, M. S.; Freedman, D. E. Forging solid-state qubit design principles in a molecular furnace. *Chem. Mater.* **2017**, *29*, 1885−1897.
(16) Coronado, E. Molecular magnetism: from chemical design to spin control in molecules, materials and devices. *Nature Reviews Materials* **2020**, *5*, 87−104.
(17) Banerjee, R. *Functional Supramolecular Materials: From Surfaces to MOFs*; The Royal Society of Chemistry, 2017.
(18) Barth, J. V.; Costantini, G.; Kern, K. Engineering atomic and molecular nanostructures at surfaces. *Nature* **2005**, *437*, 671−679.
(19) Elemans, J. A.; Lei, S.; De Feyter, S. Molecular and Supramolecular Networks on Surfaces: From Two-Dimensional Crystal Engineering to Reactivity. *Angew. Chem., Int. Ed.* **2009**, *48*, 7298−7332.
(20) Wiesendanger, R.; Güntherodt, H.-J.; Güntherodt, G.; Gambino, R.; Ruf, R. Observation of vacuum tunneling of spin-polarized electrons with the scanning tunneling microscope. *Phys. Rev. Lett.* **1990**, *65*, 247.
(21) Czerner, M.; Rodary, G.; Wedekind, S.; Fedorov, D. V.; Sander, D.; Mertig, I.; Kirschner, J. Electronic picture of spin-polarized tunneling with a Cr tip. *J. Magn. Magn. Mater.* **2010**, *322*, 1416−1418.
(22) Repp, J.; Meyer, G.; Stojković, S. M.; Gourdon, A.; Joachim, C. Molecules on insulating films: scanning-tunneling microscopy imaging of individual molecular orbitals. *Phys. Rev. Lett.* **2005**, *94*, 026803.
(23) Swart, I.; Sonnleitner, T.; Repp, J. Charge state control of molecules reveals modification of the tunneling barrier with intramolecular contrast. *Nano Lett.* **2011**, *11*, 1580−1584.
(24) Repp, J.; Meyer, G.; Olsson, F. E.; Persson, M. Controlling the charge state of individual gold adatoms. *Science* **2004**, *305*, 493−495.
(25) Kügel, J.; Karolak, M.; Senkpiel, J.; Hsu, P.-J.; Sangiovanni, G.; Bode, M. Relevance of Hybridization and Filling of 3d Orbitals for the Kondo Effect in Transition Metal Phthalocyanines. *Nano Lett.* **2014**, *14*, 3895−3902.
(26) Paul, W.; Yang, K.; Baumann, S.; Romming, N.; Choi, T.; Lutz, C. P.; Heinrich, A. J. Control of the millisecond spin lifetime of an electrically probed atom. *Nat. Phys.* **2017**, *13*, 403−407.
(27) Pacchioni, G.; Giordano, L.; Baistrocchi, M. Charging of metal atoms on ultrathin MgO/Mo (100) films. *Physical review letters* **2005**, *94*, 226104.
(28) Sterrer, M.; Risse, T.; Pozzoni, U. M.; Giordano, L.; Heyde, M.; Rust, H.-P.; Pacchioni, G.; Freund, H.-J. Control of the charge state of metal atoms on thin MgO films. *Physical review letters* **2007**, *98*, 096107.
(29) Zhang, X.; Wolf, C.; Wang, Y.; Aubin, H.; Bilgeri, T.; Willke, P.; Heinrich, A. J.; Choi, T. Electron spin resonance of single iron phthalocyanine molecules and role of their non-localized spins in magnetic interactions. *Nat. Chem.* **2022**, *14*, 59−65.
(30) Lever, A. B.; Wilshire, J. P. Electrochemistry of Iron Phthalocyanine Complexes in Nonaqueous Solvents and the Identification of Five-Coordinate Iron(I) Phthalocyanine Derivatives. *Inorg. Chem.* **1978**, *17*, 1145−1151.
(31) Hollerer, M.; Luftner, D.; Hurdax, P.; Ules, T.; Soubatch, S.; Tautz, F. S.; Koller, G.; Puschnig, P.; Sterrer, M.; Ramsey, M. G. Charge transfer and orbital level alignment at inorganic/organic interfaces: the role of dielectric interlayers. *ACS Nano* **2017**, *11*, 6252−6260.
(32) Kovarik, S.; Schlitz, R.; Vishwakarma, A.; Ruckert, D.; Gambardella, P.; Stepanow, S. Spin torque-driven electron paramagnetic resonance of a single spin in a pentacene molecule. *Science* **2024**, *384*, 1368−1373.
(33) Briganti, M.; Serrano, G.; Poggini, L.; Sorrentino, A. L.; Cortigiani, B.; de Camargo, L. C.; Soares, J. F.; Motta, A.; Caneschi, A.; Mannini, M.; Totti, F.; Sessoli, R. Mixed-Sandwich Titanium(III) Qubits on Au(111): Electron Delocalization Ruled by Molecular Packing. *Nano Lett.* **2022**, *22*, 8626−8632.
(34) Isvoranu, C.; Wang, B.; Schulte, K.; Ataman, E.; Knudsen, J.; Andersen, J. N.; Bocquet, M. L.; Schnadt, J. Tuning the spin state of iron phthalocyanine by ligand adsorption. *J. Phys.: Condens. Matter* **2010**, *22*, 472002.
(35) Noh, K.; Colazzo, L.; Urdaniz, C.; Lee, J.; Krylov, D.; Devi, P.; Doll, A.; Heinrich, A. J.; Wolf, C.; Donati, F.; Bae, Y. Template-directed 2D nanopatterning of S = 1/2 molecular spins. *Nanoscale Horiz.* **2023**, *8*, 624−631.
(36) Moreno-Pineda, E.; Martins, D. O.; Tuna, F. Electron Paramagnetic Resonance. *Royal Society of Chemistry* **2020**, *27*, 146−187.
(37) Cornia, A.; Mannini, M.; Sainctavit, P.; Sessoli, R. Chemical strategies and characterization tools for the organization of single molecule magnets on surfaces. *Chem. Soc. Rev.* **2011**, *40*, 3076−3091.
(38) Domingo, N.; Bellido, E.; Ruiz-Molina, D. Advances on structuring, integration and magnetic characterization of molecular nanomagnets on surfaces and devices. *Chem. Soc. Rev.* **2012**, *41*, 258−302.
(39) Giannozzi, P.; Baroni, S.; Bonini, N.; Calandra, M.; Car, R.; Cavazzoni, C.; Ceresoli, D.; Chiarotti, G. L.; Cococcioni, M.; Dabo, I.; et al. QUANTUM ESPRESSO: a modular and open-source software project for quantum simulations of materials. *J. Phys.: Condens. Matter* **2009**, *21*, 395502.
(40) Giannozzi, P.; Andreussi, O.; Brumme, T.; Bunau, O.; Nardelli, M. B.; Calandra, M.; Car, R.; Cavazzoni, C.; Ceresoli, D.; Cococcioni, M.; et al. Advanced capabilities for materials modelling with Quantum ESPRESSO. *J. Phys.: Condens. Matter* **2017**, *29*, 465901.
(41) Garrity, K. F.; Bennett, J. W.; Rabe, K. M.; Vanderbilt, D. Pseudopotentials for high-throughput DFT calculations. *Comput. Mater. Sci.* **2014**, *81*, 446−452.
(42) Dal Corso, A. Pseudopotentials periodic table: From H to Pu. *Comput. Mater. Sci.* **2014**, *95*, 337−350.
(43) Perdew, J. P.; Burke, K.; Ernzerhof, M. Generalized gradient approximation made simple. *Physical review letters* **1996**, *77*, 3865.
(44) Sabatini, R.; Gorni, T.; De Gironcoli, S. Nonlocal van der Waals density functional made simple and efficient. *Phys. Rev. B* **2013**, *87*, 041108.
(45) Varini, N.; Ceresoli, D.; Martin-Samos, L.; Girotto, I.; Cavazzoni, C. Enhancement of DFT-calculations at petascale: nuclear magnetic resonance, hybrid density functional theory and Car-Parrinello calculations. *Comput. Phys. Commun.* **2013**, *184*, 1827−1833.
(46) Giannozzi, P.; Baseggio, O.; Bonfà, P.; Brunato, D.; Car, R.; Carnimeo, I.; Cavazzoni, C.; De Gironcoli, S.; Delugas, P.; Ferrari Ruffino, F. Quantum ESPRESSO toward the exascale. *J. Chem. Phys.* **2020**, *152*, 154105.
(47) Mauri, F.; Louie, S. G. Magnetic Susceptibility of Insulators from First Principles. *Phys. Rev. Lett.* **1996**, *76*, 4246−4249.
(48) Bunău, O.; Calandra, M. Projector augmented wave calculation of x-ray absorption spectra at the $L_{2,3}$ edges. *Phys. Rev. B* **2013**, *87*, 205105.
(49) Gougoussis, C.; Calandra, M.; Seitsonen, A. P.; Mauri, F. First-principles calculations of x-ray absorption in a scheme based on ultrasoft pseudopotentials: From α−quartz to high-T_c compounds. *Phys. Rev. B* **2009**, *80*, 075102.

https://doi.org/10.1021/acs.jpca.4c07627
J. Phys. Chem. A 2025, 129, 2173−2181

(50) Reina Gálvez, J.; Wolf, C.; Delgado, F.; Lorente, N. Cotunneling mechanism for all-electrical electron spin resonance of single adsorbed atoms. *Phys. Rev. B* **2019**, *100*, 035411.
(51) Reina-Gálvez, J.; Lorente, N.; Delgado, F.; Arrachea, L. All-electric electron spin resonance studied by means of Floquet quantum master equations. *Phys. Rev. B* **2021**, *104*, 245435.
(52) Reina-Gálvez, J.; Wolf, C.; Lorente, N. Many-body non-equilibrium effects in all-electric electron spin resonance. *Phys. Rev. B* **2023**, *107*, 235404.
(53) Witte, G.; Lukas, S.; Bagus, P. S.; Wöll, C. Vacuum level alignment at organic/metal junctions: "Cushion" effect and the interface dipole. *Appl. Phys. Lett.* **2005**, *87*, 263502.
(54) Willenbockel, M.; Lüftner, D.; Stadtmüller, B.; Koller, G.; Kumpf, C.; Soubatch, S.; Puschnig, P.; Ramsey, M. G.; Tautz, F. S. The interplay between interface structure, energy level alignment and chemical bonding strength at organic-metal interfaces. *Phys. Chem. Chem. Phys.* **2015**, *17*, 1530−1548.
(55) Berkowitz, J. Photoelectron spectroscopy of phthalocyanine vapors. *J. Chem. Phys.* **1979**, *70*, 2819−2828.
(56) Marzouk, S.; Heinrich, B.; Lévêque, P.; Leclerc, N.; Khiari, J.; Méry, S. Phthalocyanine-based dumbbell-shaped molecule: Synthesis, structure and charge transport studies. *Dyes Pigm.* **2018**, *154*, 282−289.
(57) Evans, D. A.; Vearey-Roberts, A. R.; Roberts, O. R.; Williams, G. T.; Cooil, S. P.; Langstaff, D. P.; Cabailh, G.; McGovern, I. T.; Goss, J. P. Transport and optical gaps and energy band alignment at organic-inorganic interfaces. *J. Appl. Phys.* **2013**, *114*, 123701.
(58) Sugie, A.; Nakano, K.; Tajima, K.; Osaka, I.; Yoshida, H. Dependence of Exciton Binding Energy on Bandgap of Organic Semiconductors. The. *J. Phys. Chem. Lett.* **2023**, *14*, 11412−11420.
(59) Fukuda, T.; Kobayashi, N. *Handbook of Porphyrin Science*; World Scientific Publishing Company, 2010; pp 1−644.
(60) Haidu, F.; Fechner, A.; Salvan, G.; Gordan, O. D.; Fronk, M.; Lehmann, D.; Mahns, B.; Knupfer, M.; Zahn, D. R. T. Influence of film thickness and air exposure on the transport gap of manganese phthalocyanine. *AIP Advances* **2013**, *3*, 062124.
(61) Kumar, P.; Kumar, A.; Sreedhar, B.; Sain, B.; Ray, S. S.; Jain, S. L. Cobalt Phthalocyanine Immobilized on Graphene Oxide: An Efficient Visible-Active Catalyst for the Photoreduction of Carbon Dioxide. *Chem.—Eur. J.* **2014**, *20*, 6154−6161.
(62) Mohammed, T. H.; Eman, M. N.; Addnan, H. A.-A. Study on the UV-Visble of Ni- Phthalocyanine thin film Optical Properties. *International Journal of Thin Film Science and Technology* **2012**, *1*.
(63) Uranbileg, N.; Tsagaantsooj, T.; Enkhbayar, A.; Darambazar, D.; Erdene-Ochir, M.-E.; Chimed, G. Fabrication and Characterization of Copper Phthalocyanine- Based Field Effect Transistors. *Proceedings of the 5th International Conference on Chemical Investigation and Utilization of Natural Resource (ICCIUNR-2021)* **2021**, 9−14.
(64) Stachowiak, A.; Kedzierski, K.; Barszcz, B.; Kotwica, K.; Wrobel, D. Determination of phthalocyanines energy gaps based on spectroscopic and electrochemical studies and DFT calculations. *J. Mol. Liq.* **2021**, *341*, 116800.
(65) Grobosch, M.; Aristov, V. Y.; Molodtsova, O. V.; Schmidt, C.; Doyle, B. P.; Nannarone, S.; Knupfer, M. Engineering of the Energy Level Alignment at Organic Semiconductor Interfaces by Intramolecular Degrees of Freedom: Transition Metal Phthalocyanines. *J. Phys. Chem. C* **2009**, *113*, 13219−13222.
(66) Leuenberger, M.; Loss, D. Quantum computing in molecular magnets. *Nature* **2001**, *410*, 789−793.
(67) Bader, K.; Winkler, M.; Slageren, J. V. Tuning of molecular qubits: Very long coherence and spin-lattice relaxation times. *Chem. Commun.* **2016**, *52*, 3623−3626.
(68) Gaita-Ariño, A.; Luis, F.; Hill, S.; Coronado, E. Molecular spins for quantum computation. *Nat. Chem.* **2019**, *11*, 301−309.
(69) Vincent, R.; Klyatskaya, S.; Ruben, M.; Wernsdorfer, W.; Balestro, F. Electronic read-out of a single nuclear spin using a molecular spin transistor. *Nature* **2012**, *488*, 357−360.
(70) Godfrin, C.; Ferhat, A.; Ballou, R.; Klyatskaya, S.; Ruben, M.; Wernsdorfer, W.; Balestro, F. Operating Quantum States in Single Magnetic Molecules: Implementation of Grover's Quantum Algorithm. *Phys. Rev. Lett.* **2017**, *119*, 187702−5.
(71) Lerch, A.; Fernandez, L.; Ilyn, M.; Gastaldo, M.; Paradinas, M.; Valbuena, M. A.; Mugarza, A.; Ibrahim, A. B. M.; Sundermeyer, J.; Höfer, U.; Schiller, F. Electronic Structure of Titanylphthalocyanine Layers on Ag(111). *J. Phys. Chem. C* **2017**, *121*, 25353−25363.
(72) König, T.; Simon, G. H.; Rust, H.-P.; Heyde, M. Work Function Measurements of Thin Oxide Films on Metals—MgO on Ag(001). *J. Phys. Chem. C* **2009**, *113*, 11301−11305.
(73) Wolf, C.; Delgado, F.; Reina, J.; Lorente, N. Efficient Ab Initio Multiplet Calculations for Magnetic Adatoms on MgO. *J. Phys. Chem. A* **2020**, *124*, 2318−2327.
(74) Loth, S.; Lutz, C. P.; Heinrich, A. J. Spin-polarized spin excitation spectroscopy. *New J. Phys.* **2010**, *12*, 125021.
(75) Sabik, A.; Gołek, F.; Antczak, G. Thermal desorption and stability of cobalt phthalocyanine on Ag(100). *Appl. Surf. Sci.* **2018**, *435*, 894−902.
(76) Bodner, A.; Jeske, P.; Weyhermueller, T.; Wieghardt, K.; Dubler, E.; Schmalle, H.; Nuber, B. Mono- and dinuclear titanium(III)/titanium(IV) complexes with 1,4,7-trimethyl-1,4,7-triazacyclononane (L). Crystal structures of a compositionally disordered green and a blue form of [LTiCl3]. Structures of [LTi(O)(NCS)2], [LTi(OCH3)Br2](ClO4), and [L2Ti2(O)2F2(.mu.-F)](PF6). *Inorg. Chem.* **1992**, *31*, 3737−3748.
(77) Zhang, X.-F.; Wang, Y.; Niu, L. Titanyl phthalocyanine and its soluble derivatives: Highly efficient photosensitizers for singlet oxygen production. *J. Photochem. Photobiol., A* **2010**, *209*, 232−237.
(78) Lee, J. H.; Urdaniz, C.; Reale, S.; Noh, K. J.; Krylov, D.; Doll, A.; Colazzo, L.; Bae, Y. J.; Wolf, C.; Donati, F. Interpreting x-ray absorption spectra of vanadyl phthalocyanines spin qubit candidates using a machine learning assisted approach. *Phys. Rev. B* **2024**, *109*, 235427.
(79) Antczak, G.; Kamiński, W.; Sabik, A.; Zaum, C.; Morgenstern, K. Complex Surface Diffusion Mechanisms of Cobalt Phthalocyanine Molecules on Ag(100). *J. Am. Chem. Soc.* **2015**, *137*, 14920−14929.
(80) Phark, S. H.; Chen, Y.; Bui, H. T.; Wang, Y.; Haze, M.; Kim, J.; Bae, Y.; Heinrich, A. J.; Wolf, C. Double-Resonance Spectroscopy of Coupled Electron Spins on a Surface. *ACS Nano* **2023**, *17*, 14144−14151.
(81) Bruker Almanac 2010. https://www.pascal-man.com/pulseprogram/Almanac2010.pdf, pp 47 −50 (accessed 2024/11/03).
(82) Shehada, S.; dos Santos Dias, M.; Guimarães, F. S. M.; Abusaa, M.; Lounis, S. Trends in the hyperfine interactions of magnetic adatoms on thin insulating layers. *npj Computational Materials* **2021**, *7*, 87.
(83) Jauho, A. P.; Wingreen, N. S.; Meir, Y. Time-dependent transport in interacting and noninteracting resonant-tunneling systems. *Phys. Rev. B* **1994**, *50*, 5528−5544.
(84) Arrachea, L.; Moskalets, M. Relation between scattering-matrix and Keldysh formalisms for quantum transport driven by time-periodic fields. *Phys. Rev. B* **2006**, *74*, 245322.
(85) Lorente, N.; Reina-Gálvez, J.; Wolf, C.; Switzer, E. D. TimeESR: An STM-ESR code solving a QME in the time domain. https://github.com/qphensurf/TimeESR 2022; (Accessed on 2024/12/12).
(86) Wolf, C.; Heinrich, A. J.; Phark, S.-h. On-Surface Atomic Scale Qubit Platform. *ACS Nano* **2024**, *18*, 28469−28479.
(87) Zhang, X., Reina-Gálvez, J.; Wu, D.; Martinek, J.; Heinrich, A. J.; Choi, T.; Wolf, C. Electric field control of the exchange field of a single spin impurity on a surface. *arXiv* 2024; https://arxiv.org/abs/2412.03866.

https://doi.org/10.1021/acs.jpca.4c07627
J. Phys. Chem. A 2025, 129, 2173−2181